ARTICLE

pubs.acs.org/Biomac

Photobactericidal Porphyrin-Cellulose Nanocrystals: Synthesis, Characterization, and Antimicrobial Properties

Elke Feese,[†] Hasan Sadeghifar,[‡,#] Hanna S. Gracz,[§] Dimitris S. Argyropoulos,[†,‡,∥] and Reza A. Ghiladi*[,†]

[†]Departments of Chemistry, [‡]Forest Biomaterials, and [§]Molecular and Structural Biochemistry, North Carolina State University, Raleigh, North Carolina, United States

[∥]Department of Chemistry, University of Helsinki, Helsinki, Finland

[#]Department of Wood and Paper Science, Islamic Azad University, Chalous, Iran

Supporting Information

ABSTRACT: Adherence and survival of pathogenic bacteria on surfaces leading to concomitant transmission to new hosts significantly contributes to the proliferation of pathogens, which in turn considerably increases the threat to human health, particularly by antibiotic-resistant bacteria. Consequently, more research into effective surface disinfection and alternative materials (fabrics, plastics, or coatings) with antimicrobial and other bioactive characteristics is desirable. This report describes the synthesis and characterization of cellulose nanocrystals that were surface-modified with a cationic porphyrin. The porphyrin was appended onto the cellulose surface via the Cu(I)-catalyzed Huisgen−Meldal−Sharpless 1,3-dipolar cycloaddition having occurred between azide groups on the cellulosic surface and porphyrinic alkynes. The resulting, generally insoluble, crystalline material, CNC-Por (**5**), was characterized by infrared and diffusion ^{1}H NMR spectroscopies, gel permeation chromatography, and thermogravimetric analysis. Although only suspended, and not dissolved, in an aqueous system, CNC-Por (**5**) showed excellent efficacy toward the photodynamic inactivation of *Mycobacterium smegmatis* and *Staphylococcus aureus*, albeit only slight activity against *Escherichia coli*. The synthesis, properties, and activity of CNC-Por (**5**) described herein serve as a benchmark toward our overall objectives of developing novel, potent, bioactive, photobactericidal materials that are effective against a range of bacteria, with potential utilization in the health care and food preparation industries.

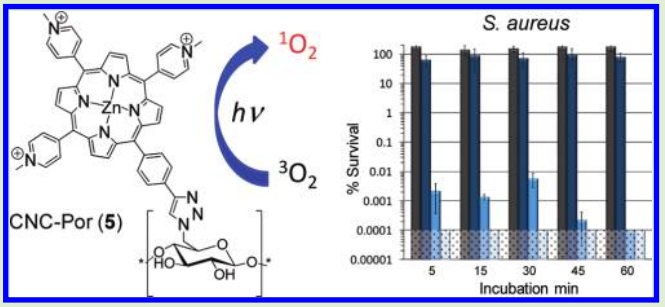

Hospital acquired infections, in particular, highlight the issue of adherence and survival of bacteria on surfaces leading to an increase in the proliferation and transmission of bacteria. Specifically, antibiotic-resistant bacteria are a rising threat to human health. According to the Centers of Disease Control and Prevention, about 1.7 million healthcare associated infections cause upward of 99000 deaths annually in the United States.[1] A total of 5−10% of all hospitalized patients are adversely affected, which in turn is adding about $30−45 billion to health care costs annually.[2] Food processing/packaging, food service, and wastewater treatment industries, as well as personal households, are also areas of concern and can contribute to the spread of disease through contaminated or improperly disinfected surfaces. Consequently, more research into effective surface disinfection and alternative materials (fabrics, plastics, or coatings) with antimicrobial properties is needed. Several classes of antimicrobial agents are currently being investigated or are commercially available, among which are polymeric compounds containing quarternary ammonium,[3−7] pyridinium[8,9] or phosphonium salts,[5,10] N-halamines,[11,12] biguanides,[13] antibiotics,[14] heavy metals such as Ag,[14−16] and phenol derivatives.[14] Disadvantages of currently available materials are the loss of antimicrobial activity by leaching of the biocide in noncovalent systems, consumption of the germicidal ability, environmentally hazardous agents, or dependency on direct contact of the antimicrobial entity with the microorganism. Thus, there is an urgent need for the development of novel materials with the potential capability of rapid, efficient, and low-cost sterilization of a range of bacteria.

During the past few decades, photodynamic inactivation (PDI) has garnered the attention of many researchers as an alternative technique for eradicating microorganisms. Therefore, we see great potential in the development of photobactericidal materials that could satisfy many desired characteristics while overcoming some of the shortcomings of currently available antimicrobial materials. PDI employs a localized, light-activated photosensitizer (PS) that generates cytotoxic species, particularly singlet oxygen, upon illumination with visible light. Singlet oxygen, as opposed to some common disinfectants such as chlorine and hypochlorite, can be regarded as an environmentally benign germicide (short lifetime of 10^{-6} s in water[17] and

Received: May 27, 2011
Revised: August 3, 2011
Published: August 12, 2011

Scheme 1. Synthesis of Cellulose Nanocrystal-Porphyrin Conjugate CNC-Por (5)

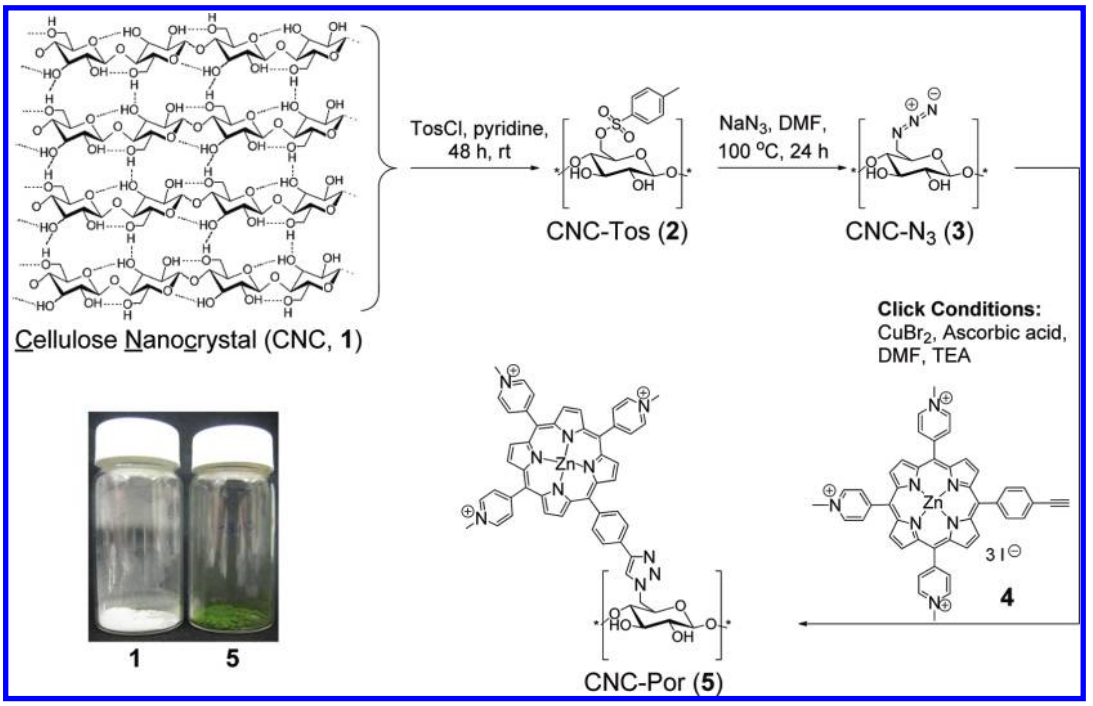

reverting back to harmless ground state oxygen if unreacted). Singlet oxygen is known to be able to diffuse over significant distances, as long as 100−200 nm in water and about 1 mm in air.[18] Bezman et al. were the first to demonstrate this by photodynamic inactivation of *E. coli* with Rose Bengal immobilized on polystyrene beads.[19] Dahl et al. demonstrated the successful photodynamic inactivation of *Salmonella lyphimurium* and *E. coli* by the flow of singlet oxygen through a 0.65 mm air gap between the microbes and a photosensitizer.[20] The feasibility of the concept of a "photobactericidal surface" is further supported by studies showing that the photosensitizers retain their ability to reduce a bacterial cell count when adsorbed, codissolved and casted, as well as covalently bound, to nanoparticles,[21,22] polymers,[23,24] films,[25−27] or membranes.[28] Of particular interest for our work is a series of studies by Krausz and co-workers who have investigated the incorporation of selected porphyrin photosensitizers into cellulose esterified plastic films and demonstrated the photobactericidal activity of such films.[26,27,29]

Cellulose is Earth's most abundant natural biopolymer, consisting of high molecular weight β-1,4-linked anhydro-D-glucose polymer chains, and therefore, in our eyes, an excellent starting material for developing new, more sustainable materials from renewable resources.[30,31] Distortions in the hydrogen bonding of the tightly cross-linked chain packing causes amorphous regions within the otherwise crystalline microfibrils. Acidic hydrolysis of these defects results in rod-shaped cellulose nanocrystals [CNC (**1**), Figure SD1] with high mechanical strength and etched, chemically modifiable, molecular surface patterns.[31−33] For example, these nanomaterials are rigid rods, with embedded chirality, and a unique etched nanopattern composed of primary hydroxymethyl groups on their surface that may readily be further functionalized for the purposes of anchoring a variety of molecules onto them.[33] Furthermore, these nanomaterials, being of a carbohydrate nature, are of inherent compatibility with biological tissue and, therefore, of unique utility with respect to their bioavailability, biocompatibility, and biodegradability considerations.

Consequently, the focus of the present report is the surface modification of cellulose nanocrystals CNC (**1**) with the cationic porphyrin (Por) **4**, yielding the conjugate CNC-Por (**5**) (Scheme 1). The advantages of a covalent attachment of the porphyrin to the surface of the cellulose nanocrystals potentially include conferring longer lasting or permanent antimicrobial properties to the cellulose (improved durability), minimizing the leaching of the biocidal agent into the surrounding environment, and prevention of porphyrin aggregation. The covalent attachment of **4** to **1** was achieved via the Cu(I)-catalyzed Huisgen−Meldal−Sharpless 1,3-dipolar cylcoaddition (hereafter referred to as an example of a "Click reaction") between an azide on the CNC surface and the alkyne-containing porphyrin.[34,35] To the best of our knowledge, this work is among the first attempts to covalently append cationic porphyrins to the surface of cellulose nanocrystals. The physicochemical characteristics of CNC-Por (**5**) were investigated using a combination of spectroscopic and chemical analyses, thereby demonstrating the covalent linkage between the two moieties, while its photobactericidal characteristics were also investigated. As will be shown, CNC-Por (**5**) was highly efficient in mediating the photodynamic inactivation of *M. smegmatis* and *S. aureus*, and did exhibit some activity against *E. coli*. The potential and the significance of CNC-Por (**5**) in the context of cellulose-derived antimicrobial fabrics is highlighted by the fact that *S. aureus* has been found to be able to survive for weeks under dry conditions on cotton fabrics used in hospital environments.[36,37] As such, we see possibilities for the incorporation of photosensitizer-modified-cellulose nanocrystals into paper, fabrics and plastics, thereby creating novel, biodegradable, photobactericidal materials from renewable sources

that may be capable of sterilizing a range of bacteria with high efficacy, rapidly, and at minimal cost.

MATERIALS AND METHODS

Materials. Buffer salts were purchased from Fisher Scientific, Middlebrook 7H9 agar and 7H10 broth from BD Difco, LB broth Miller from EMD Chemicals and Tryptic Soy Broth from Teknova. Unless otherwise specified, all other chemicals were obtained from commercial sources in the highest purity available. Ultrapure water used for all media and buffers was provided by an Easypure II system (Barnstead). UV−visible absorption measurements were performed on a Varian Cary 50 Bio instrument or a Genesys 10 UV scanning spectrophotometer from Thermo Electron Corp for single wavelength measurements. All procedures were carried out under commonly practiced sterile techniques. A Perkin-Elmer Model 3110 atomic absorption spectrometer was used for the determination of the Zn ion content of **5**. FT-IR (Fourier transform infrared) spectra were measured on a Thermo Nicolet NEXUS 670 FT-IR spectrophotometer. Spectra in the range of 4000−650 cm^{-1} were obtained with a resolution of 4 cm^{-1} by accumulating 64 scans. Thermal decomposition temperatures were determined using a TA Instrument TGAQ500 ramping 10 °C/min under N_2 purging. CNC samples were dried using a lyophilizing system from Labconco (Kansas City, Mo, USA). For Transmission Electron Microscopy (TEM), a suspension (0.01% w/v in water) of cellulose nanocrystals were deposited as drops on carbon-coated electron microscope grids, negatively stained with uranyl acetate, and allowed to dry. The grids were observed with a Philips 400T microscope operated at an accelerating voltage of 120 kV.

Formation of Cellulose Nanocrystals, CNC (1). The cellulose nanocrystals employed in this study were formed by acidic hydrolysis as reported in the literature with only minor modification.[33,38,39] Briefly, 2.0 g of cellulose pulp were obtained from Whatman #1 filter paper (98% α-cellulose, 80% crystallinity) and blended in a 10 Speed Osterizer Blender. Hydrolysis of the resulting pulp was achieved after 3 h at 100 °C using 100 mL of 2.5 M HBr and intermittent ultrasonication (5 min per hour, 50% power, Omni Ruptor 250 W ultrasonic homogenizer). After dilution with deionized water, the mixture was subjected to five washing/centrifugation cycles (5000*g*, 10 min, IEC Centra-CL3 Series) to remove excess acid and water-soluble fragments. Once pH 4−5 was reached, the fine cellulose particles started to disperse into the aqueous supernatant. The polydisperse cellulose contained in the turbid supernatant was collected and subjected to centrifugation at 15,000*g* for 60 min in a Sorvall Superspeed centrifuge to remove ultrafine particles. The sediment containing the cellulose nanocrystals with an average length of 100−400 nm was dried using a lyophilizing system, yielding 0.9 g CNC (**1**; 47% yield).

Surface Tosylation of Cellulose Nanocrystals Yielding CNC-Tos (2). Surface-tosylated CNC was synthesized analogous to the method described by Rahn et al.[40] 0.5 g of CNC (**1**; 4 mmol glucosyl units) was suspended in pyridine (10 mL) and the mixture was cooled to 10 °C. Tosyl chloride (0.9 g, 5 mmol) was then added, and the reaction mixture was stirred for 2 days at room temperature. Addition of 100 mL of ethanol to the reaction mixture resulted in a precipitate that was collected by filtration. The product was washed with ethanol (50 mL) and deionized water (50 mL) five times each and freeze-dried, yielding 0.585 g CNC-Tos (**2**).

Surface Azide Bearing CNC-N_3 (3). Synthesis of the azide surface-modified cellulose nanocrystals, CNC-N_3 (**3**), was conducted according to literature procedures with some modifications.[33,41−43] A total of 400 mg CNC-Tos (**2**) was suspended in 20 mL of DMF (*N*,*N*-dimethylformamide), followed by careful addition of 400 mg sodium azide. The reaction mixture was stirred at 100 °C for 24 h. After precipitation through the addition of 50 mL of deionized water and centrifugation, the product was washed five times with ethanol (50 mL) and five times with deionized water (50 mL). The resulting product was dialyzed against deionized water for 3 days and, consequently, freeze-dried to yield 330 mg CNC-N_3 (**3**; 84%). The degree of substitution (DS) was calculated from the elemental analysis (C 41.06%, H 6.35%, O 48.84%, N 3.75%) DS = 0.14.

Click Reaction of CNC-N_3 (3) with Porphyrin (4). Conditions for the Cu(I)-catalyzed Huisgen−Meldal−Sharpless 1,3-dipolar cycloaddition reaction were selected from the literature.[33,35,42,44,45] A total of 400 mg of CNC-N_3 (**3**) and 400 mg of porphyrin **4** were mixed in 30.0 mL of DMF (99.5% purity). A mixture of 30 mg $CuBr_2$, 70 mg ascorbic acid, and 200 μL of triethylamine in 1 mL of DMF was then added, and the reaction mixture was stirred vigorously for 5 min at room temperature, followed by stirring at 60 °C for 36 h. The product was isolated by centrifugation and washed three times with ethanol and three times with water (50 mL each time). For subsequent characterization and the photodynamic inactivation studies, the CNC-Por material was divided into ∼100 mg aliquots, and each aliquot was further washed to remove any unreacted porphyrin **4** (4 × 15 mL with DMF, 3 × 15 mL with 0.05 M acetic acid, 4 × 15 mL with water, and 3 × 15 mL with ethanol). After washing, the final product was isolated by 60 min centrifugation at 12000*g* and freeze-dried, yielding 480 mg of CNC-Por (**5**) material.

Acetylation of CNC-N_3 (3) and CNC-Por (5). For the PFGSE-NMR (pulsed field gradient spin echo nuclear magnetic resonance) spectroscopic studies, samples of CNC-N_3 (**3**) and CNC-Por (**5**) were acetylated to generate DMSO-soluble derivatives according to literature procedure with minor modification.[46−48] A total of 100 mg of the CNC-derivative was dissolved in 3 g 1-allyl-3-methylimidazolium chloride (about 3% w/w) at 80 °C for 12 h. Acetic anhydride (315 μL; 5 mol/mol anhydrous glucose units) was added to the solution, and the mixture was stirred for 2 h at 80 °C. The product was precipitated by addition of 30 mL of deionized water and washed seven times with water. The CNC-derivative was obtained after freeze-drying and residual water was removed under high vacuum.

Benzoylation of CNC-N_3 (3) and CNC-Por (5). A total of 50 mg of either CNC-N_3 (**3**) or CNC-Por (**5**) was dissolved in 1-allyl-3-methylimidazolium chloride (950 mg) in a 15 mL flask by first thoroughly dispersing the sample, followed by heating at 80 °C with magnetic stirring until the solution was transparent (about 4 h). Pyridine (330 μL, 3.7 mmol) was added, and the mixture was homogenized to form a uniform paste before being allowed to cool to room temperature. Benzoyl chloride (380 μL, 3.3 mmol) was then added in one portion, and the sample was subsequently stirred for 3 h at room temperature. The benzoylated product was precipitated by the addition of a 1:3 mixture of deionized water and EtOH with vigorous stirring for 5 min, after which the precipitate was collected by filtration using a medium porosity sintered glass funnel. The collected material was washed with EtOH and triturated with MeOH at room temperature for 18 h. The final product was collected by filtration and dried under vacuum to yield a green powder.

Gel Permeation Chromatography. GPC analysis was carried out with a Waters model ALC/GPC 204 (Waters Associates, Milford, MA) and 510 pump equipped with a UV detector (210 nm). The analysis was conducted at 40 °C using THF as the eluent at a flow rate of 0.7 mL/min. A total of 200 μL of a 1 mg/mL solution of the analyte in THF was injected onto two Ultrastyragel columns (Styragel HR 1 and Styragel HR 5E, Waters) connected in series for analysis. Standard monodisperse polystyrenes (molecular weight ranges from 0.82 to 1860 kg/mol) were used for calibration. The number (M_n) and weight (M_w) average molecular weights were calculated using the Millenium 32 software.

Determination of Porphyrin Loading in CNC-Por (5) by Atomic Absorption Spectroscopy. Atomic absorption spectroscopy

was used to determine the concentration of Zn ions in samples of CNC-Por (**5**), which is equivalent to the porphyrin loading if complete metalation of the porphyrin is assumed. About 10 mg of lyophilized CNC-Por (**5**) was suspended in 10 mL of 1 M HCl in a volumetric flask. The solution was heated to 60 °C for 2 h resulting in demetalation of the porphyrin. The zinc ion concentration was determined using the standard addition method: To each sample for the calibration curve (range of 0.01−0.1 mmol/L $Zn(OAc)_2$ in 1 M HCl), 1 mL of the demetalated CNC-Por stock solution was added for a total volume of 10 mL. Under these conditions, the response of the atomic absorption instrument containing a Zn lamp operated at 10 mA was linear. The zinc ion concentration of the sample was calculated from the *Y*-intercept and the slope of the calibration curve. Typical porphyrin loadings were in the range of 0.16 ± 0.03 μmol porphyrin/mg of CNC-Por (**5**). Determination of the Zn content was done in triplicate for each batch of **5** synthesized.

Pulsed-Field-Gradient, Spin−Echo NMR Spectroscopy.[49,50] Modification of the glucose−OH groups by acetylation rendered the resulting CNC-Por compound sufficiently soluble in DMSO-d_6 to conduct NMR spectroscopic studies. Spectra were obtained on a Bruker Avance 500 MHz spectrometer (1996) with an Oxford Narrow Bore Magnet (1989), Dell Host Workstation, and Red Hat Linux operation system with Topspin 2.1 software. The instrument was equipped with three-channel gradient control (GRASPIII), variable-temperature-, precooling-, temperature stabilization, as well as three frequency channels with waveform memory and amplitude shaping units. ^{1}H NMR (proton nuclear magnetic resonance spectroscopy) diffusion measurements were conducted with a 5 mm triple axis gradient probe (ID500−5EB, Nalorac Cryogenic Corp) equipped with actively shielded gradient coils. The gradient strength was calibrated using literature values for water diffusion in $^1H_2O/^2H_2O$ mixtures. The longitudinal eddy current (LED) pulse sequence was used in all diffusion experiments.[51,52] A total of 10 gradient experiments were acquired for each data set. The gradient strength was adjusted linearly from 5.3 to 47.7 G/cm and applied in the *y*-direction, while all other delays were held constant. The gradient pulse interval Δ was 10 ms, the gradient duration δ 5 ms, with a recovery time of 6 ms. Acquisition temperature was 24.5 °C. The attenuation of the signal intensities derived from the peak height of each experiment was used to generate Stejskal−Tanner plots to determine the diffusion coefficients. Diffusion coefficients were estimated by least-squares regression.

Preparation of Photosensitizer Stock Solutions. Stock solutions (1 mM) of photosensitizers in filter-sterilized ultrapure water were prepared based on the porphyrin content determined by atomic absorption spectroscopy, in the case of CNC-Por (**5**), and stored in the dark at −80 °C. At the concentrations employed, turbidity of CNC-Por (**5**) solutions was noted.

Bacterial Strains and Growth Conditions. The bacterial strains *Mycobacterium smegmatis* mc^2 155 (donated by Prof. William Jacobs, Albert Einstein College of Medicine, U.S.A.), *Escherichia coli* BL21-(Dε3)pLysS (Strategene, U.S.A.) and *Staphylococcus aureus* 29213 (donated by Prof. Christian Melander, North Carolina State University, U.S.A.) were used in this study. *M. smegmatis* was grown in 5 mL cultures in Middlebrook 7H9 media with ADS (albumin dextrose saline) and 100 μg/mL cycloheximide as the antibiotic.[53] *E. coli* was cultured in Miller's LB Broth with 50 μg/mL chloramphenicol and 100 μg/mL ampicillin. *S. aureus* was grown in 5 mL cultures in Tryptic Soy Broth without antibiotics. The cells were incubated at 37 °C on an orbital shaker (500 rpm) until an optical density (OD_{600}) of 0.65−0.70 (*M. smegmatis* and *S. aureus*) or 0.33−0.40 (*E. coli*) at 600 nm, corresponding to a concentration of 1−3 × 10^8 CFU/mL, was reached (CFU = colony forming units from a single bacterial cell).

Incubation of Cells with Photosensitizer. The 5 mL culture with a concentration of 1−3 × 10^8 CFU/mL was pelleted by centrifugation (10 min, 3716*g*) at room temperature, the supernatant discarded, and the cells were resuspended in a total volume of 5 mL of PBS (phosphate buffered saline = 170 mM NaCl, 3.4 mM KCl, 10 mM Na_2HPO_4, 1.8 mM KH_2PO_4, pH 7.2 with additional 0.05% Tween 80) and the appropriate volume of the photosensitizer stock solution. The cells were incubated between 5 and 60 min in the dark and agitated by a vortex mixer set to the lowest speed. No degradation of CNC-Por (**5**) was observed in PBS solution over the time range examined in this study.

Cell Illumination Conditions. All photosensitization experiments were performed using a noncoherent light source, PDT light model LC122 (LumaCare, U.S.A.), and the fluence rate was measured with an Orion power meter (Orphir Optronics Ltd., Israel). Aliquots (1 mL) of the cell suspension in PBS were added to a sterile 24-well plate (BD Falcon, flat bottom) and illuminated with visible light (400−700 nm) with a fluence rate of 60 mW/cm^2 for the duration of 15 or 30 min (corresponding to fluences of 54 or 108 J/cm^2) while magnetically stirred. Tween-80 (0.05%) was added to the buffer to prevent excessive aggregation of the PS during the illumination process. After illumination, an aliquot was used for viability assays. All experiments were conducted in triplicate at a minimum.

Cell Survival Assays. A total of 40 μL from the illuminated cell suspension was 1:10 serially diluted six times and plated on square plates (Middlebrook 7H10-ADS solid media for *M. smegmatis*, Miller's LB Broth−Agar plates for *E. coli* and Tryptic Soy Broth−Agar plates for *S. aureus*), as described by Jett and co-workers.[54] The plates were incubated at 37 °C in the dark for 48−60 h (*M. smegmatis*) or overnight (*E. coli* and *S. aureus*). The survival rate was determined from the ratio of CFU/mL of the illuminated solution and the dark control. Due to the plating technique employed, a maximum of a six log unit change in CFU/mL corresponding to ≥100 CFU/mL could be detected for an initial concentration of 1 × 10^8 CFU/mL. Survival rates of <0.0001% could not be detected. The percentage of survival for samples for which the corresponding plates did not show any colonies was thus set to the detection limit of 0.0001%. Samples with photosensitizer present but kept in the dark (dark control) and illuminated samples with CNC-N_3 (**3**) present (light control) served as controls. Statistical significance was assessed via a two-tailed, unpaired Student's *t* test.

RESULTS

Synthesis. The cationic water-soluble ethynylphenyl porphyrin **4** was synthesized in four steps. Briefly, the porphyrin macrocyle was synthesized from 4-pyrindinecarboxaldehyde, 4-[(trimethylsilyl)ethynyl]benzaldehyde, and pyrrole under mildly acidic catalysis in refluxing fresh xylenes. The desired A_3B porphyrin was isolated from the statistical mixture of porphyrins by column chromatography. Following ethyne deprotection in a methanol/THF (1:4) solution in the presence of 1 equiv potassium carbonate, metalation of the porphyrin macrocycle was accomplished with zinc acetate in THF/MeOH. Quarternization of the amine nitrogen of the pyridine substituents was performed with iodomethane in DMF at elevated temperature. Full experimental details will be published elsewhere.

The nanocrystalline cellulose material employed in this study, CNC (**1**), was obtained by acid hydrolysis of cotton fibers. Such treatment causes selective degradation of amorphous cellulosic regions producing defect-free, rod-like crystals with a length of 100−400 nm (Figure SD1). Cellulose pulp from cotton filter paper (Whatman #1, 98% cellulose, 80% crystallinity) was treated with 2.5 M HBr and intermittent ultrasonication for optimized high yields of cellulose nanocrystals according to literature procedure.[33,55] The CNCs were isolated and purified by a series of centrifugation and washing steps.

Modification of the primary hydroxyl groups of the CNC for the installment of surface-azide groups was successful in two

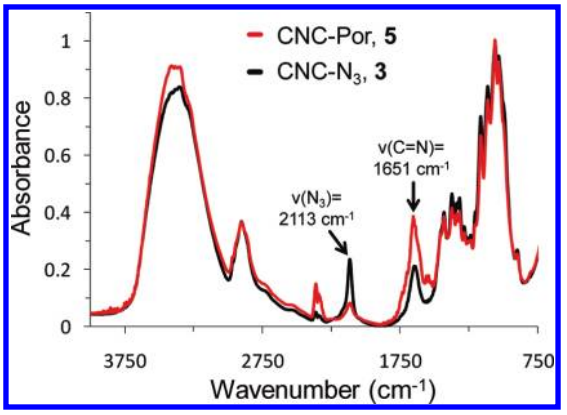

Figure 1. IR spectra of CNC-N_3 (**3**) and CNC-Por (**5**).

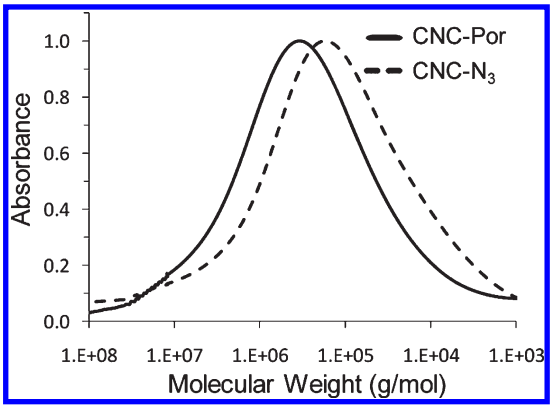

Figure 2. Gel permeation chromatographs of benzoylated derivatives of CNC-N_3 (**3**) and CNC-Por (**5**) in THF.

steps (Scheme 1). First, CNC (**1**) was suspended in pyridine and treated with tosyl chloride, yielding the surface-tosylated cellulose analog **2**. FTIR spectroscopy revealed that, in addition to the typical absorption bands of the cellulose backbone, new vibrational modes assigned to the aromatic ring (1596, 1495, and 815 cm^{-1}) and SO_2 [1363 (antisymmetric) and 1175 (symmetric) cm^{-1}, Figure SD2] stretching modes appeared, verifying successful tosylate modification. The tosyl substituents were subsequently displaced by azide groups using sodium azide in a DMF suspension, yielding CNC-N_3 (**3**). The azide-modified CNC-N_3 (**3**) exhibited a new stretching band characteristic for the azide moiety at 2113 cm^{-1}, with concomitant loss of the vibrational modes associated with the tosylated precursor **2**. Elemental analysis of CNC-N_3 (**3**) revealed a nitrogen content of 3.75%. Taking the molecular weight of the anhydrous glucose unit of 162 g/mol and nitrogen (14 g/mol) into account, the degree of methylhydroxy substitution (DS) with surface azide groups was calculated as DS = (0.0375 × 162)/(3 × 14) = 0.14. The theoretical maximum of surface available primary hydroxyl groups can be determined from the following parameters: The average dimensions (8.6 × 7.7 nm) of the CNC rectangular rods have been determined by X-ray crystallography.[55] Thus, the amount of individual cellulose chains within a cotton crystallite can be calculated using the two lattice parameters of the cellulose I_β unit cell, a = 0.61 nm and b = 0.54 nm, respectively.[56,57] Based on this model, the planes corresponding to 0.61 nm are parallel to the long side (C_1 = 8.6 nm) of the rectangular whisker section whereas the 0.54 nm are parallel to the short side (C_2 = 7.7 nm).[58,59] Thus, within this average crystal, there are (8.6 × 7.7)/(0.61 × 0.54) = 201 cellulose chains. At the surface, this corresponds to 2 × (8.6/0.54) + 2 × (7.7/0.61) = 57 cellulose chains. The ratio of surface chains to the total number of chains within the crystals is therefore 0.29. Due to the 2-fold screw axis of the glucose units within each chain, a maximum degree of primary hydroxyl groups on the surface of the CNC (**1**) is about 0.29/2 = 0.145. When compared to the experimentally determined DS of 0.14 in CNC-N_3 (**3**), the two-step azide substitution was highly efficient, converting >95% of the available surface methylhydroxy groups.

Appendage of the porphyrin onto the cellulose nanocrystalline surface was achieved by the Cu(I)-catalyzed Huisgen−Meldal−Sharpless 1,3-dipolar cycloaddition reaction.[35,42,45,60,61] Several conditions, including temperature (room temperature to 60 °C), solvents (EtOH, DMF), and Cu catalysts (CuI, $CuBr_2$/ascorbate, $[Cu(OTf)]_2 \cdot tol$), were surveyed, and $CuBr_2$ in combination with ascorbate in DMF at elevated temperature in the presence of triethylamine proved to give the most optimal results. The choice of DMF as the solvent was based upon the solubility of the porphyrin **4**. Purification of the resulting product, an insoluble green crystalline material [(**5**), Scheme 1], was achieved by careful washing and centrifugation to remove both unreacted **4** and copper catalyst per literature precedent.[62,63]

IR Characterization of CNC-Por (5). Clear evidence for the successful reaction of the ethyne functional group in **4** with the azide containing cellulose nanocrystals **3** was obtained from IR spectroscopic analysis (Figure 1). The IR spectrum of the azide surface-modified cellulose, CNC-N_3 (**3**; black trace), clearly exhibited an azide band at 2113 cm^{-1}, which is within the range of 2160−2080 cm^{-1} expected for the antisymmetric azide stretching motion.[64] Upon reaction with the ethyne containing porphyrin **4**, the azide band in the IR spectrum of the resulting product **5** was diminished by 72%. Additionally, an intensity increase of the bands in the region around 1651 cm^{-1} indicated the presence of C═N double bonds arising from the porphyrin and triazole linkage. The broad band centered around 1647 cm^{-1} in the spectrum for the CNC-N_3 (**3**) is most likely due to the bending motion of adsorbed water and overlaps with the C═N stretching modes for CNC-Por (**5**).[65]

Molecular Weight Determination and Porphyrin Loading of CNC-Por (5). The molecular weight gain attributable to the appended porphyrins was assessed by gel permeation chromatography (GPC). Due to the insolubility of cellulosic samples in organic solvents, the hydroxyl groups were benzoylated prior to GPC analysis. Samples of **3** and **5** were dissolved in the ionic liquid 1-allyl-3-methylimidazolium chloride and treated with benzoyl chloride. The weight average molecular weight (M_w), number average molecular weight (M_n), and consequently the distribution of molecular weight also known as polydispersity (M_w/M_n) were calculated from the GPC data. The molecular weight distribution of **5** clearly shifted to higher molecular weights with 102000 g/mol representing the weight average molecular weight (M_w) compared to 69000 g/mol (M_w) for **3** (Figure 2, Table 1). This 48% increase in the M_w further supports the notion of a covalent appendage between the porphyrin **4** and CNC-N_3 (**3**). Further, we have attributed the increase in polydispersity (M_w/M_n) of the benzoylated CNC-Por sample when compared to that of the benzoylated CNC-N_3 material, to a distribution of surface-bound porphyrins arising from the partial

Table 1. Molecular Weight Distributions of Benzoylated Derivatives of CNC-N_3 (3) and CNC-Por (5) in THF

	weight average molecular weight (M_w) 10^3 g/mol	number average molecular weight (M_n) 10^3 g/mol	polydispersity (M_w/M_n)
CNC-N_3 (3), benzoylated	69	19.7	3.5
CNC-Por (5), benzoylated	102	17.6	5.8

reaction of **4** with **3** (Table 1). From the molecular weight increase between CNC-N_3 (**3**) and CNC-Por (**5**) and considering the average formula mass of the anhydrous glucose-N_3 unit of 166 g/mol, we were able to estimate the porphyrin loading of the CNCs as one porphyrin molecule per 15 glucose molecules. Considering the degree of substitution of DS = 0.14 for the azide groups on the crystal surface, we estimate that approximately 50% of the azide groups were reacted with the cationic porphyrin, corresponding to an overall degree of substitution of DS = 0.07 for the porphyrin.

Alternatively, the porphyrin loading was determined indirectly by measuring the Zn-ion content by atomic absorption spectroscopy of a CNC-Por (**5**) sample in 1 M HCl using the standard addition method.[66] Under the assumption that one Zn-ion detected corresponds to one porphyrin molecule covalently attached to the cellulose nanocrystalline surface, a maximum loading of $\sim 0.16 \pm 0.03$ μmol porphyrin/mg **5** was obtained. Using this method, the porphyrin loading was determined as 1 porphyrin per $\sim$20 glucose units.

Pulsed Field Gradient Spin Echo ^{1}H NMR Spectroscopy. NMR spectroscopic characterization of CNC-Por (**5**) proved to be possible only upon acetylation due to the insolubility of this crystalline material in common solvents. Briefly, CNC-Por (**5**) was dissolved in 1-allyl-3-methylimidazolium chloride (AMIM-Cl) at 80 °C over 12 h and, subsequently, reacted with acetic anhydride. The resulting acetylated CNC-Por was rendered soluble in DMSO and, therefore, was amenable for characterization by NMR spectroscopy. The ^{1}H NMR spectrum of acetylated **5** revealed the presence of proton resonances for cellulose along side with those of the porphyrin component. However, relative to the cellulose, the small concentration of the porphyrin (approximately 1 molecule/15−20 glucose units), which had only been appended to the surface of the cellulose nanocrystals, did not allow for any further conclusions regarding the covalent conjugation between the two entities. Therefore, pulsed field gradient spin echo ^{1}H NMR experiments (PFGSE-LED pulse sequence) were performed.[49,52,67] The PFGSE-NMR technique allows for the determination of diffusion coefficients even for mixtures of compounds.[68] Diffusion NMR, with its ability to draw conclusions about molecular size, shape, aggregation, or binding in complex solutions, has proven useful in a range of different fields such as bioanalytical, pharmaceutical, environmental, and materials chemistry.[69−74] In pulsed field gradient experiments, a magnetic gradient pulse whose strength varies throughout the sample is applied in addition to the static magnetic field. Thereby, it is possible to label the spins according to their translational position in the NMR tube. After this encoding pulse, the molecules are allowed to diffuse for a specified time period, after which a decoding gradient pulse is applied. If diffusion to a different part of the sample has occurred, the decoding pulse will not completely reverse the phase change of the encoding pulse, and an attenuation of the NMR signal is observed. The change in resonance intensity for simple PFG pulse sequences is proportional to the diffusion coefficient (D) and square of the gradient pulse amplitude (G), as described in eq 1:

$$I = I_0 \exp[-D(G\delta\gamma)^2(\Delta - \delta/3)] \quad (1)$$

in which I_0 denotes the signal intensity in the absence of a gradient pulse, δ the gradient duration, γ the magnetogyric ratio of the nucleus under investigation, and Δ the settling time. A plot of $\ln(I/I_0)$ over G^2 allows determination of D from the slope.[75]

Figure 3A shows the results of the pulsed field gradient spin echo ^{1}H NMR experiments with the acetylated compound **5**. The aromatic resonances of the porphyrin moiety were found from 8.0 to 9.5 ppm, whereas those from the methyl groups of the *N*-methylpyridinium substituents showed a signal at 4.7 ppm. The proton signals for the acetylated cellulose backbone appeared at $\sim$2 ppm (acetyl groups) and between 3.5 and 5.2 ppm (cellulose backbone). A small attenuation of the signal intensity for the cellulose backbone of **5** was observed by increasing the gradient strength incrementally. Magnification of the aromatic porphyrin region around 8−9 ppm also exhibited an equally small change in signal intensity (Figures 3A and SD3). This indicated that both the porphyrin and the acetylated cellulose diffused at the same rate (estimated diffusion coefficient $D = 2 \times 10^{-7}$ cm^2/s, Table 2) and, therefore, strongly suggested that they were covalently connected. As a control experiment, Figure 3B shows the results for the PFGSE-^{1}H NMR spectroscopic studies of a mixture of the porphyrin **4** and acetylated CNC-N_3 (**3**). A faster loss in signal intensity for the porphyrin protons (i.e., δ 9.4 or 4.7 ppm as representative resonances, Figure SD3) when compared to the methyl groups of the acetylated CNC-N_3 (**3**; δ 2.0 ppm) was noted. The respective diffusion coefficients estimated from the NMR data differ by an order of magnitude, with 2×10^{-6} cm^2/s for the porphyrin **4** and 3×10^{-7} cm^2/s for the acetylated CNC-N_3, whereas the diffusion rates for acetylated CNC-Por and CNC-N_3 were very similar (Table 2). Taken together, the results of the PFGSE-^{1}H NMR spectroscopic studies strongly suggest the presence of a covalent bond, and not adventitious binding, between the porphyrin macrocycle and the cellulose nanocrystal in CNC-Por (**5**).

Thermogravimetric Analysis of CNC-Por (5). In our efforts to further confirm and elucidate the physicochemical characteristics of these novel materials, we also investigated the thermal behavior of the starting materials, porphyrin **4** and CNC-N_3 (**3**) versus that of CNC-Por (**5**) by thermogravimetric analysis (Figure 4). The 5% weight losses for both porphyrin **4** and CNC-N_3 (**3**) were observed at 235 and 285 °C, respectively. For CNC-Por (**5**), a different thermal gravimetric behavior was apparent. Two degradation profiles were observed, with minor degradation commencing around 210 °C (weight loss of 20%) and major decomposition above 320 °C. This difference in thermal behavior further supports our claim that the CNC-N_3 (**3**) had been chemically modified upon a coupling reaction with the porphyrin **4**, producing a covalent linkage between the two.

Photodynamic Inactivation Studies with CNC-Por (5). The ability of CNC-Por (**5**) to inactivate *E. coli*, *M. smegmatis*, and *S. aureus* was evaluated. The bacteria were grown to a concentration of $\sim 10^8$ colony forming units per mL (CFU/mL), resuspended in PBS-0.05% Tween-80 containing buffer, incubated with the

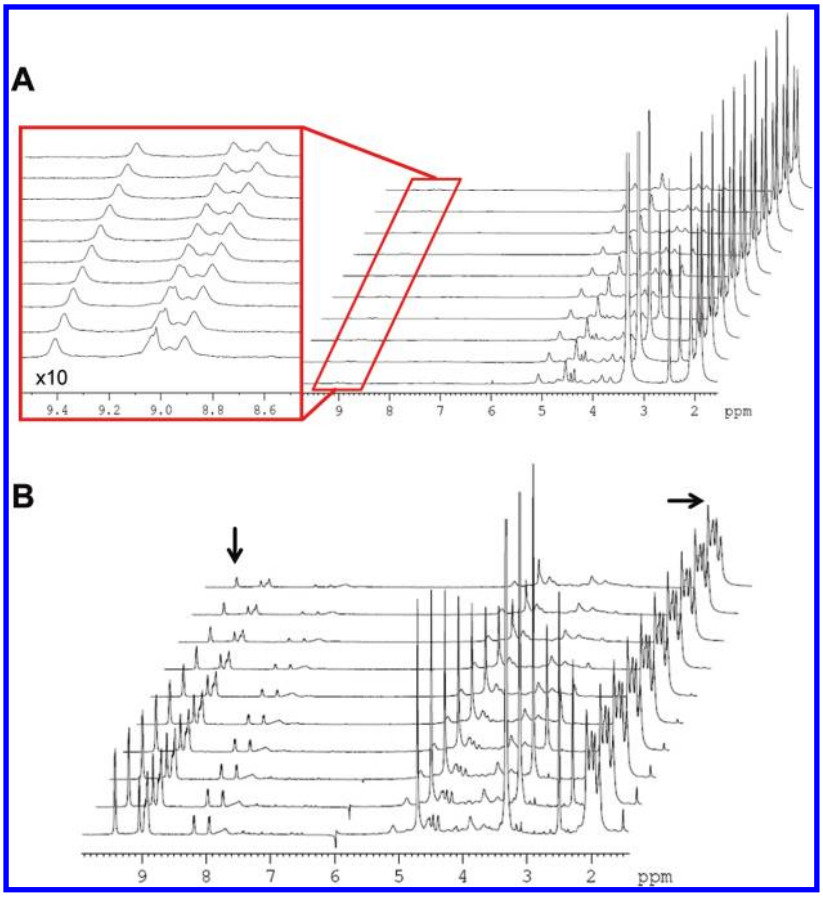

Figure 3. Pulsed field gradient spin echo ^{1}H NMR in DMSO-d_6 of (A) acetylated CNC-Por, and (B) control experiments with a mixture of porphyrin **4** and acetylated CNC-N_3. The indicated signals were used for the estimation of diffusion coefficients.

Table 2. Estimated Diffusion Coefficients (D) Determined from PFGSE-^{1}H NMR Spectroscopy

compound	fragment	δ (ppm)	D (cm^2/s)
CNC-Por (**5**, acetylated)	porphyrin	9.4	2×10^{-7}
	cellulose	2.1	2×10^{-7}
CNC-N_3 (**3**, acetylated)	porphyrin	9.4	2×10^{-6}
mixture with porphyrin **4**	cellulose	2.1	3×10^{-7}

photosensitizer in the dark (incubation time was varied from 5 to 60 min) and subsequently illuminated with white light (400−700 nm) with a fluence rate of 60 mW/cm^2 for 15 or 30 min (equivalent to a fluence of 54 or 108 J/cm^2). The stock solution for **5** was prepared based on the porphyrin loading determined by atomic absorption spectroscopy, and concentrations listed hereafter refer to the concentration of porphyrin on **5** present in the suspension. The concentration dependence of the CNC-Por (**5**) photosensitizer for *S. aureus* and *M. smegmatis* at fixed incubation (30 min) and illumination times (15 min) is illustrated in Figure SD4, and suggested a 20 μM concentration of the PS for these studies. Control experiments included monitoring of cell survival in PBS buffered solution in the dark, PS treatment of the bacteria in the dark, and light exposure of bacterial suspensions to azide surface-modified cellulose (Table SD1). The percentage of survival was determined by the ratio of the colony count from illuminated and nonilluminated control cell suspensions.

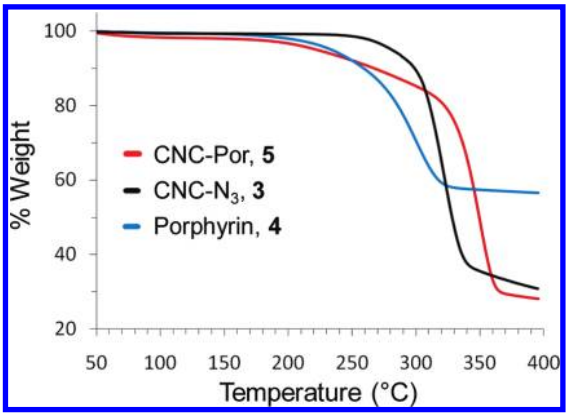

Figure 4. Thermal gravimetric analysis of CNC-Por (**5**).

The results for light-treated samples as well as dark controls are shown in Figure 5. Of the three bacteria examined, the Gram-negative *E. coli* appeared to be the least susceptible to photodynamic inactivation by CNC-Por (**5**) at a porphyrin concentration of 20 μM (Figure 5A). No statistically significant inactivation of *E. coli* was observed with 15 min illumination time under all incubation periods tested ($P > 0.2$). With longer illumination times (30 min) a 1−2 log unit reduction in the cell count was observable ($P = 0.05$ for 45 and 60 min incubation time). The dark incubation time before the illumination step did not appear to play

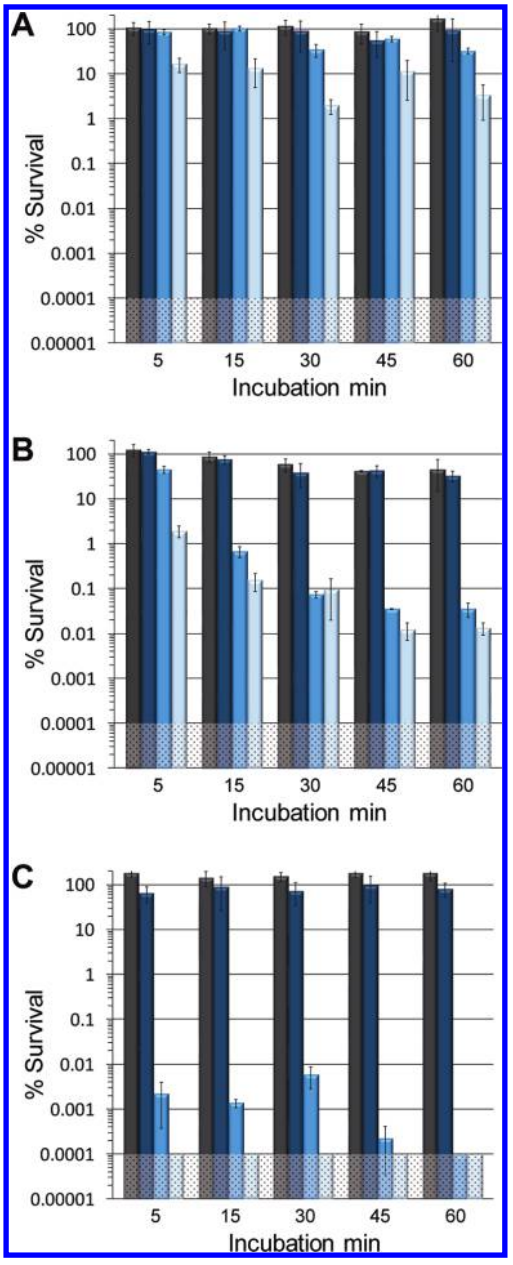

Figure 5. Photodynamic inactivation of (A) *E. coli*, (B) *M. smegmatis*, and (C) *S. aureus* using 20 μM CNC-Por (**5**) as the photosensitizer. The dark incubation time was varied over 5, 15, 30, 45, and 60 min. Displayed is the % survival in PBS buffered bacterial suspensions (black rectangle), CNC-Por dark control (navy blue rectangle) and light-treated samples after illumination times of 15 (sky blue rectangle) or 30 (light blue rectangle) min (total fluences of 54 and 108 J/cm^2, respectively, at 60 mW/cm^2). As the plating technique employed to determine % survival did not allow for detection of survival rates of <0.0001%, data points below the detection limit are set to 0.0001% survival for graphing purposes. The shaded areas correspond to undetectable cell survival with the assay employed.

a significant role, although there was a slight improvement of ~0.5 log units in the inactivation of *E. coli* for incubation times of at least 30 min. Dark controls containing CNC-Por (**5**) showed no toxicity toward *E. coli*.

For PDI of *M. smegmatis*, no dark toxicity was apparent for the CNC-Por photosensitizer (Figure 5B). For long dark incubation times (i.e., 60 min), a reduction of the cell count to about 30% was observed for both the bacteria-only and CNC-Por dark controls, which was most likely due to the lack of nutrients in the PBS buffered solutions. Upon illumination for 15 min, *M. smegmatis* was found to be more susceptible to photodynamic inactivation by CNC-Por (**5**) than *E. coli*. Clear loss in viable cells was observed starting with 2 log units for 15 min incubation time and increased to 3.5 log units after a 60 min incubation for the same light dose (P = 0.003). When the illumination time was increased to 30 min, a greater impact on the inactivation of the bacterium was observed, with approximately 1% survival of *M. smegmatis* being observed after only 5 min incubation time (P = 0.03). For longer incubation times (≥45 min), this doubling of the light dose also resulted in improved efficacy, with a statistically significant survival rate of ~0.01% (P < 0.01; ~4 log units reduction in viable cells). Additionally, a clear dependency of cell survival on the PS incubation time was apparent for *M. smegmatis*. This observation was unusual when compared to other studies with soluble photosensitizers: PS are generally thought to quickly bind to the bacterium, and therefore no differences in PDI for different incubation times have been typically observed.[76−79]

Photodynamic inactivation of *S. aureus* using CNC-Por (**5**) was also found to be highly efficient (Figure 5C). Whereas *M. smegmatis* and *E. coli* both contain an outer cell membrane for enhanced protection,[80−82] *S. aureus* is classified as a Gram-positive bacterium with an easily penetrated cell envelope lacking an outer cell membrane. Therefore, significant vulnerability to singlet oxygen and other reactive species produced in the photosensitizer mediated process was expected. At 20 μM concentration of CNC-Por (**5**), short incubation times of 5−15 min were sufficient for a viable cell reduction of an impressive 5 log units after 15 min illumination (P = 0.003). For all samples illuminated for 30 min, no CFUs were detected, and survival rates were therefore below the detection limit of <0.0001%.

As shown in Table SD1, the presence of azide surface-modified cellulose nanocrystals **3** did not significantly affect the survival of any of the bacterial strains investigated after illumination for 15 or 30 min. Therefore, any loss in the viable cell count can be attributed to the photosensitizing action of the porphyrin incorporated into compound **5** if the levels of unbound porphyrin impurity are negligible. As outlined in the experimental, the CNC-Por material used for photodynamic inactivation experiments was carefully and extensively washed with DMF, 0.05 M acetic acid, ultrapure water, and ethanol to remove any adventitiously bound ethynylphenyl porphyrin **4** from the cellulose−porphyrin conjugate (**5**). Despite this treatment, however, UV−visible spectroscopic analysis of the supernatant of the CNC-Por stock solution revealed the presence of a putatively dissolved porphyrin species of up to 88 nM based on the 20 μM CNC-Por suspension employed in the above PDI experiments. Thus, the question arises as to whether this was indicative of the presence of unreacted and adventitiously bound **4** in the cellulosic material, and consequently, the PDI results noted above were derived from this solution-based PS impurity, or whether the "dissolved" porphyrin was actually finely suspended **5**. Therefore, to rule out the possibility that the photodynamic inactivation results were mediated by unreacted porphyrin rather than CNC-Por (**5**), PDI studies were performed for all three bacteria using the water-soluble ethynylphenyl porphyrin **4** as the photosensitizer for comparison (Table 3). As *S. aureus* was susceptible to significant photodynamic inactivation by **4** at concentrations as low as even 10 nM, with a 5 log unit reduction

Table 3. Results of PDI Studies with the Water-Soluble Porphyrin 4 as a Function of Different Bacteria, [PS], and Light Dose

		% survival[a,b]	
bacterium	concentration, nM	15 min illumination	30 min illumination
E. coli	100	0.0021 ± 0.0015	0.0003 ± 0.0002
	50	24.65 ± 15.80	0.0644 ± 0.0582
M. smegmatis	100	46.64 ± 5.10	14.71 ± 4.72
S. aureus	100	0.0002 ± 0.0002	0.00009 ± 0.00009
	50	0.0006 ± 0.0003	0.00003 ± 0.00002
	10	0.14 ± 0.01	0.003 ± 0.001

[a] Samples were incubated for 5 min in the dark before illumination. [b] Illumination with white light (400−700 nm, 60 mW/cm^2).

($P < 0.001$) noted for 30 min illumination, this result alone cannot rule out that adventitiously bound **4** was responsible for the PDI results above given that a similar reduction in viable cells was noted for **5** under identical conditions. However, *M. smegmatis* could only be inactivated by **4** by at most 1 log unit at 100 nM concentration and 30 min illumination ($P < 0.001$), which contrasts markedly with the ∼4 log unit reduction mediated by **5** under these conditions. Even more critically, however, is that *E. coli* exhibited a 3−4 log unit reduction in cell viability after 30 min of illumination ($P < 0.001$) at 50 nM **4**, whereas **5** was unable to inactivate *E. coli* by more than 1 log unit when subjected to the same PDI conditions. These latter two results with *M. smegmatis* and *E. coli* strongly suggest that the PDI results noted above for CNC-Por (**5**) were directly attributable to the bound porphyrin of the cellulose-porphyrin conjugate, and not due to the presence of adventitiously bound/unreacted **4** as an impurity.

DISCUSSION

Only a few examples of porphyrin−cellulose conjugates can be found in the literature. Most of these employed esterified cellulose as a backbone that can be cast into a plastic film with limited thermal stability.[26,27,29,83,84] Krausz and co-workers have appended neutral, anionic, and cationic porphyrins to cellulose esters as well as to cotton fabric and were able to demonstrate the photobactericidal activity of the materials.[26,27,29,85−87] More recently, they have also reported in a conference paper the synthesis and characterization of polyaminated chlorin *p6* tethered to cellulose nanocrystals (via ionic and covalent attachment), and investigated this system for antitumor activity.[88] In our work, we have also selected the well characterized crystalline nanocellulose system as the polymeric backbone. Cellulose nanocrystals offer a particular degree of molecular control for precise functionalization due to their rigidity, defined surface structure and dimensions, all of which are not offered by the amorphous cellulose esters. Additionally, cellulose nanocrystals are readily biodegradable and, as a renewable resource, provide an excellent starting material for the systematic investigation of cellulose−porphyrin conjugates and their interactions with microbes in order to develop new advanced materials with photobactericidal activity.

Herein, we describe the successful synthesis, characterization, and photodynamic inactivation study for the porphyrin−cellulose nanocrystalline conjugate CNC-Por (**5**) against three types of bacteria. We developed a synthetic strategy which produces cellulose nanocrystalline materials with covalently surface appended photosensitizers with potential use in papers or cotton fabrics. Specifically, the ethyne containing porphyrin **4** and azide surface modified cellulose **3** moieties were joined using the Cu(I)-catalyzed Huisgen−Meldal−Sharpless 1,3-dipolar cycloaddition. Using infrared and diffusion NMR spectroscopies and supported by gel permeation chromatography and thermogravimetric analysis, the covalent linkage between the porphyrin and the cellulose was clearly demonstrated. In the future, the modular approach of Click reactions may enable us to append an array of ethyne-containing porphyrins to cellulose nanocrystals, and the resulting conjugates can consequently be screened for their ability to inactivate bacteria.

The porphyrin loading on the cellulose surface was determined from independent samples from the molecular mass increase measured by gel permeation chromatography of benzoyl-derivatized **5**, as well as by measurement of the zinc-ion content of **5** by atomic absorption spectroscopy. The loading was found to be in the range of one porphyrin molecule per 15−20 glucose units. Consequently, the maximum degree of substitution with porphyrin based on the surface available hydroxyl groups was calculated as DS = 0.07. Based upon the azide surface modification of DS = 0.14, about 50% of all azide groups successfully reacted with the porphyrin **4**, explaining the residual azide band observed in the IR spectrum of **5** (Figure 1). Possible explanations for the partial substitution include CNC aggregation during the Cu(I)-catalyzed Huisgen−Meldal−Sharpless 1,3-dipolar cycloaddition reaction, which would leave some sites inaccessible for reaction, or a steric argument where surface-crowding, exacerbated by the electrostatic repulsion between the positively charged porphyrin moieties, results in the incomplete reaction of the azide groups. Strategies for increased surface loading could involve spacer units, thereby imparting the conjugated molecules more spatial flexibility. The spacer could be incorporated in the porphyrin as a longer chain tether with terminal alkyne, or as a tether with a terminal azide linked to the cellulose surface. In a related system, Krausz and co-workers observed increased porphyrin loadings for porphyrin-cellulose-laurate esters if a spacer of 11 carbons instead of 4 were installed on the porphyrin (estimated as DS = 0.19, however, not a surface reaction).[27]

Our detailed photodynamic inactivation experiments show the potential of CNC-Por (**5**) as a photosensitizer on solid support. The degree of bacterial inactivation varied vastly over the conditions and the three different classes of bacteria [*E. coli* (Gram-negative), *S. aureus* (Gram-positive), and *M. smegmatis* (mycobacterium)] investigated. PS-mediated inactivation was observed ranging from 2 log units reduction for *E. coli* (60 min incubation, 30 min illumination, 99% cell loss, $P = 0.05$) to 6 log units reduction for *S. aureus* (5 min incubation, 30 min illumination, 99.9999% cell loss, $P = 0.03$). Compared to using dissolved PS for photodynamic inactivation experiments, a 100−500-fold increase in porphyrin concentration was needed to affect photodynamic inactivation with the insoluble compound **5**.[89] Nevertheless, this supports the idea that direct binding and uptake of the photosensitizer are not necessary requirements for photodynamic inactivation, and that the production of singlet oxygen in close proximity to the bacteria can also result in cellular death.[18−20] *S. aureus* appeared to be the most susceptible bacterium for photodynamic inactivation, which is reasonable

considering the comparably permeable cell wall of Gram-positive bacteria.[90] Even lowering of the concentration to 5 μM porphyrin on **5** still allowed ~1 log inactivation after incubation and illumination for 15 min each ($P = 0.003$, Figure SD4). The highest viable cell loss observed for *E. coli*, for comparison, was only about 99% ($P = 0.05$). We suggest that the additional permeation barrier (outer cell membrane) of this Gram-negative bacterium is responsible for the much lower inactivation rates observed.[80] Although *M. smegmatis* does retain the Gram stain and, therefore, should be considered Gram-positive, the mycobacterial cell envelope contains elements of both Gram-positive and negative bacteria.[81] In addition, genome analysis indicates that mycobacteria might be more closely related to Gram-negative rather than Gram-positive bacteria.[82] Regardless, the unusually low cell wall permeability is undisputed and is the major reason for the relatively high resistance of mycobacteria to dry conditions, alkali, chemical disinfectants, therapeutic agents, and their remarkable ability to survive these hostile conditions.[81,91] Despite the impermeable cell wall, we report here efficient inactivation of *M. smegmatis* with **5** at 20 μM concentration (based upon the porphyrin content). We even observed significantly improved (1−2 log units, depending on the conditions) inactivation when compared to *E. coli*.

Control experiments with the soluble porphyrin **4** (Table 3) indicate that levels of >100 nM for *M. smegmatis*, 50 nM for *E. coli*, and 10 nM for *S. aureus* in solution would significantly reduce the viable cell count. Therefore, the presence of unbound porphyrin needed to be addressed when evaluating the data shown in Figure 5. UV−visible spectroscopic analysis of the supernatant of the CNC-Por (**5**) stock solution used in PDI experiments isolated by centrifugation (16000*g*, 30 min) showed the presence of supposedly dissolved porphyrin species. According to this analysis, at most 88 nM porphyrin species were present in the supernatant in a typical PDI experiment, part of which may be attributed to unbound porphyrin. By comparison, 100 nM of **4** caused a reduction in viable cells of less than 1 log unit against *M. smegmatis*, while at 20 μM CNC-Por (**5**) caused reductions in viable cells of up to 3−4 log units. Therefore, we can exclude unbound porphyrin as a significant contributor to the cell loss. For *E. coli*, we expect >3 log units of inactivation (30 min illumination) if CNC-Por (**5**) indeed was contaminated with 50−100 nM of **4**, but photodynamic inactivation with 20 μM **5** was ≤2 log units. Consequently, we conclude that levels of unbound porphyrin contamination must be well below 50 nM, and the porphyrin species detected in the supernatant was most likely due to small crystals of **5** that did not separate under the centrifugation conditions used. *S. aureus* was extremely sensitive to photodynamic inactivation with **4**. Even at 10 nM of **4**, a viable cell loss of 3 log units (15 min illumination) was observed. In this case, we cannot conclusively exclude the possibility that <50 nM of **4** may have partially contributed to the loss in cell viability observed during photodynamic inactivation with **5**.

Interestingly, a dependence of the degree of cell survival on the dark incubation time was apparent for *M. smegmatis*. Generally, it is agreed that the incubation time for dissolved PS does not influence the degree of bacterial inactivation because binding of the PS to the bacterial cell is fast.[76−79] Therefore, our finding is unusual and might be explained with the possible presence of endogenous mycobacterial cellulases. Cellulases are a class of enzymes whose function it is to hydrolyze cellulose.[92−95] Part of this enzyme class are endoglucanases, which are capable of interrupting the hydrogen-bonding network of crystalline cellulose leading to the separation of the individual cellulose strands, while exoglucanases hydrolyze the cellulose strands into smaller units of 2−4 glucose molecules. Whereas functional cellulases have been discovered in *Mycobaterium tuberculosis*,[96] a gene encoding functional cellulase has been identified for *M. smegmatis* (strain mc^2 155) and other mycobacteria.[97] If *M. smegmatis* expresses extracellular cellulases, these enzymes might be able to partially degrade the photosensitizer **5**, releasing smaller soluble units into the medium, which could be responsible for the observed increase of photodynamic inactivation with prolonged incubation times. Similar incubation time dependencies were not clearly observed when analyzing the PDI data for *E. coli* and *S. aureus* (Figure 5A,C). Currently, we cannot exclude that similar incubation time dependencies exist at higher concentrations of **5** for *E. coli* and lower concentrations for *S. aureus*. However, to the best of our knowledge, *E. coli* and *S. aureus* are not known to express cellulases. More detailed studies are currently under way in our laboratory to address these questions.

CONCLUSION

We have developed a synthetic route for the selective and reproducible surface modification of cellulose nanocrystals with porphyrins using the Cu(I)-catalyzed Huisgen−Meldal−Sharpless 1,3-dipolar cycloaddition reaction. The benchmark compound CNC-Por (**5**) was characterized by infrared and PFGSE-^{1}H NMR spectroscopies of the acetylated derivative, as well as size exclusion chromatographic (benzoylated **5**) and thermogravimetric analyses as proof of the covalent linkage between the porphyrin and the cellulose polymer. Promising results were obtained in our investigation of the ability of **5** to photoinactivate bacteria. Three genera of bacteria, *S. aureus* (Gram-positive), *E. coli* (Gram-negative), and *M. smegmatis* (mycobacterium), were investigated. Five-six log units reduction in viable cells were observed against *S. aureus*, 3−4 log units for *M. smegmatis*, and 1−2 log units for *E. coli* using CNC-Por (**5**) in suspension at 20 μM solution (based on the porphyrin concentration). Given the advantages of employing well-defined and uniform cellulose nanocrystals as the scaffold, future studies may allow us to systematically further investigate and understand the interaction between the porphyrin-cellulose photosensitizer and microbes in order to design PS that will be useful in photobactericidal materials. With cellulose as a biodegradable as well as renewable resource, along with the defined character and molecular control exhibited by the nanocrystalline cellulose surface, we anticipate value in the development of such cellulose−porphyrin conjugates for use in photobactericidal papers, fabrics, and coatings for applications in the healthcare and food preparation industries.

ASSOCIATED CONTENT

Supporting Information. Results of the light control experiments with azide surface-modified CNC-N_3 (Table SD1), TEM image of CNC (**1**; Figure SD1), IR spectra of CNC (**1**), CNC-Tos (**2**), and CNC-N_3 (**3**; Figure SD2), graphical representation of the loss in proton signal intensity for PFGSE-^{1}H NMR experiments (Figure SD3), and the concentration dependence of PDI for *M. smegmatis* and *S. aureus* using CNC-Por (**5**) at constant incubation and illumination

times (Figure SD4). This material is available free of charge via the Internet at http://pubs.acs.org.

AUTHOR INFORMATION

Corresponding Author
*Tel.: (919) 513-0680. Fax: (919) 515-8920. E-mail: reza_ghiladi@ncsu.edu.

ACKNOWLEDGMENT

This project was supported with funds from North Carolina State University (R.A.G and D.S.A.) as well as funds from the Finnish Funding Agency for Technology and Innovation; Tekes (D.S.A.).

REFERENCES

(1) Klevens, R. M.; Edwards, J. R.; Richards, C. L.; Horan, T. C.; Gaynes, R. P.; Pollock, D. A.; Cardo, D. M. *Public Health Rep.* **2007**, *122*, 160–166.
(2) Scott, R. D. The direct medical costs of healthcare-associated infections in U.S. hosptials and the benefits of prevention. *CS200891-A*; Centers for Disease Control and Prevention: Atlanta, GA, 2009; p 13.
(3) Sauvet, G.; Fortuniak, W.; Kazmierski, K.; Chojnowski, J. *J. Polym. Sci., Part A: Polym. Chem.* **2003**, *41*, 2939–2948.
(4) Vigo, T. L. Advances in antimicrobial polymers and materials. In *Biotechnology and Bioactive Polymers*; Gebelein, C. G., Carraher, C. E., Eds.; Plenum Press: New York, 1994; p 225.
(5) Kenawy, E.-R.; Abdel-Hay, F. I.; El-Shanshoury, A. E.-R. R.; El-Newehy, M. H. *J. Polym. Sci., Part A: Polym. Chem.* **2002**, *40*, 2384–2393.
(6) Kurt, P.; Wood, L.; Ohman, D. E.; Wynne, K. J. *Langmuir* **2007**, *23*, 4719–4723.
(7) Cen, L.; Neoh, K. G.; Kang, E. T. *Langmuir* **2003**, *19*, 10295–10303.
(8) Krishnan, S.; Ward, R. J.; Hexemer, A.; Sohn, K. E.; Lee, K. L.; Angert, E. R.; Fischer, D. A.; Kramer, E. J.; Ober, C. K. *Langmuir* **2006**, *22*, 11255–11266.
(9) Viscardi, G.; Quagliotto, P.; Barolo, C.; Savarino, P.; Barni, E.; Fisicaro, E. *J. Org. Chem.* **2000**, *65*, 8197–8203.
(10) Kanazawa, A.; Ikeda, T. *Coord. Chem. Rev.* **2000**, *198*, 117–131.
(11) Liang, J.; Chen, Y.; Ren, X.; Wu, R.; Barnes, K.; Worley, S. D.; Broughton, R. M.; Cho, U.; Kocer, H.; Huang, T. S. *Ind. Eng. Chem. Res.* **2007**, *46*, 6425–6429.
(12) Eknoian, M. W.; Worley, S. D.; Bickert, J.; Williams, J. F. *Polymer* **1999**, *40*, 1367–1371.
(13) Bromberg, L.; Hatton, T. A. *Polymer* **2007**, *48*, 7490–7498.
(14) Vigo, T. L., Antimicrobial fibers and polymers. In *Manmade Fibers: Their Origin and Development*; Seymour, R. B., Porter, R. S., Eds.; Elsevier: Amsterdam, 1992; p 214.
(15) Estevao, L. R. M.; Mendonca-Hagler, L. C. S.; Nascimento, R. S. V. *Ind. Eng. Chem. Res.* **2003**, *42*, 5950–5953.
(16) Ignatova, M.; Labaye, D.; Lenoir, S.; Strivay, D.; Jerome, R.; Jerome, C. *Langmuir* **2003**, *19*, 8971–8979.
(17) Merkel, P. B.; Kearns, D. R. *J. Am. Chem. Soc.* **1972**, *94*, 7244–7253.
(18) Midden, W. R.; Wang, S. Y. *J. Am. Chem. Soc.* **1983**, *105*, 4129–4135.
(19) Bezman, S. A.; Burtis, P. A.; Izod, T. P. J.; Thayer, M. A. *Photochem. Photobiol.* **1978**, *28*, 325–329.
(20) Dahl, T. A.; Robert Midden, W.; Hartman, P. E. *Photochem. Photobiol.* **1987**, *46*, 345–352.
(21) Lucas, R.; Granet, R.; Sol, V.; Morvan, C. L.; Policar, C.; Riviere, E.; Krausz, P. *e-Polym.* **2007**, *89*, 1–8.
(22) Carvalho, C. M. B.; Alves, E.; Costa, L.; Tome, J. P. C.; Faustino, M. A. F.; Neves, M. G. P. M. S.; Tome, A. C.; Cavaleiro, J. A. S.; Almeida, A.; Cunha, A.; Lin, Z.; Rocha, J. *ACS Nano* **2010**, *4*, 7133–7140.
(23) Wilson, M. *Infect. Control Hosp. Epidemiol.* **2003**, *24*, 782–784.
(24) Sherrill, J.; Michielsen, S.; Stojiljkovic, I. *J. Polym. Sci., Part A: Polym. Chem.* **2003**, *41*, 41–47.
(25) Bonnett, R.; Buckley, D. G.; Burrow, T.; Galia, A. B. B.; Saville, B.; Songca, S. P. *J. Mater. Chem.* **1993**, *3*, 323–324.
(26) Krouit, M.; Granet, R.; Krausz, P. *Bioorg. Med. Chem.* **2008**, *16*, 10091–10097.
(27) Krouit, M.; Granet, R.; Krausz, P. *Eur. Polym. J.* **2009**, *45*, 1250–1259.
(28) Bonnett, R.; Krysteva, M. A.; Lalov, I. G.; Artarsky, S. V. *Water Res.* **2006**, *40*, 1269–1275.
(29) Krouit, M.; Granet, R.; Branland, P.; Verneuil, B.; Krausz, P. *Bioorg. Med. Chem. Lett.* **2006**, *16*, 1651–1655.
(30) French, A. D.; Bertoniere, N. R.; Brown, R. M.; Chanzy, H.; Gray, D.; Hattori, K.; Glasser, W. *Kirk-Othmer Encyclopedia of Chemical Technology*, 5th ed.; John Wiley & Sons, Inc.: New York, 2004; Vol. 5.
(31) Habibi, Y.; Lucia, L. A.; Rojas, O. J. *Chem. Rev.* **2010**, *110*, 3479–3500.
(32) Ranby, B. G. *Discuss. Faraday Soc.* **1951**, *11*, 158–164.
(33) Filpponen, I.; Argyropoulos, D. S. *Biomacromolecules* **2010**, *11*, 1060–1066.
(34) Rostovtsev, V. V.; Green, L. G.; Fokin, V. V.; Sharpless, K. B. *Angew. Chem., Int. Ed.* **2002**, *41*, 2596–2599.
(35) Tornoe, C. W.; Christensen, C.; Meldal, M. *J. Org. Chem.* **2002**, *67*, 3057–3064.
(36) Cimolai, N. *Eur. J. Clin. Microbiol. Infect. Dis.* **2008**, *27*, 481–493.
(37) Neely, A. N.; Maley, M. P. *J. Clin. Microbiol.* **2000**, *38*, 724–726.
(38) Araki, J.; Wada, M.; Kuga, S.; Okano, T. *J. Wood Sci.* **1999**, *45*, 258–261.
(39) Araki, J.; Wada, M.; Kuga, S.; Okano, T. *Colloids Surf., A* **1998**, *142*, 75–82.
(40) Rahn, K.; Diamantoglou, M.; Klemm, D.; Berghmans, H.; Heinze, T. *Angew. Makromol. Chem.* **1996**, *238*, 143–163.
(41) Tim, L.; Claudia, H.; Thomas, H. *Macromol. Rapid Commun.* **2006**, *27*, 208–213.
(42) Zhang, J.; Xu, X.-D.; Wu, D.-Q.; Zhang, X.-Z.; Zhuo, R.-X. *Carbohydr. Polym.* **2009**, *77*, 583–589.
(43) Heinze, T.; Liebert, T. *Prog. Polym. Sci.* **2001**, *26*, 1689–1762.
(44) Hasegawa, T.; Umeda, M.; Numata, M.; Fujisawa, T.; Haraguchi, S.; Sakurai, K.; Shinkai, S. *Chem. Lett.* **2006**, *35*, 82–83.
(45) Hasegawa, T.; Umeda, M.; Numata, M.; Li, C.; Bae, A.-H.; Fujisawa, T.; Haraguchi, S.; Sakurai, K.; Shinkai, S. *Carbohydr. Res.* **2006**, *341*, 35–40.
(46) Cao, Y.; Wu, J.; Meng, T.; Zhang, J.; He, J.; Li, H.; Zhang, Y. *Carbohydr. Polym.* **2007**, *69*, 665–672.
(47) Wu, J.; Zhang, J.; Zhang, H.; He, J.; Ren, Q.; Guo, M. *Biomacromolecules* **2004**, *5*, 266–268.
(48) Schlufter, K.; Schmauder, H.-P.; Dorn, S.; Heinze, T. *Macromol. Rapid Commun.* **2006**, *27*, 1670–1676.
(49) Stejskal, E. O.; Tanner, J. E. *J. Chem. Phys.* **1965**, *42*, 288–292.
(50) Morris, K. F.; Johnson, C. S. *J. Am. Chem. Soc.* **1992**, *114*, 3139–3141.
(51) Zeng, L.; Stejskal, E. O. *Appl. Spectrosc.* **1996**, *50*, 1402–1407.
(52) Gibbs, S. J.; C. S. Johnson, J. *J. Magn. Reson.* **1991**, *93*, 395–402.
(53) Larsen, M. Some common methods in mycobacterial genetics. In *Molecular Genetics of Mycobacteria*; Hatfull, G. F., Ed.; ASM Press: Washington, DC, 2000; pp 313−320.
(54) Jett, B. D.; Hatter, K. L.; Huycke, M. M.; Gilmore, M. S. *BioTechniques* **1997**, *23*, 648–650.
(55) Filpponen, I. The Synthetic Strategies for Unique Properties in Cellulose Nanocrystals Materials; North Carolina State University: Raleigh, NC, 2009.
(56) Sugiyama, J.; Vuong, R.; Chanzy, H. *Macromolecules* **1991**, *24*, 4168–4175.
(57) Elazzouzi-Hafraoui, S.; Nishiyama, Y.; Putaux, J.-L.; Heux, L.; Dubreuil, F.; Rochas, C. *Biomacromolecules* **2008**, *9*, 57–65.

(58) Okita, Y.; Saito, T.; Isogai, A. *Biomacromolecules* **2010**, *11*, 1696–1700.
(59) Nishiyama, Y.; Langan, P.; Chanzy, H. *J. Am. Chem. Soc.* **2002**, *124*, 9074–9082.
(60) Liebert, T.; Hänsch, C.; Heinze, T. *Macromol. Rapid Commun.* **2006**, *27*, 208–213.
(61) Iha, R. K.; Wooley, K. L.; Nystrom, A. M.; Burke, D. J.; Kade, M. J.; Hawker, C. J. *Chem. Rev.* **2009**, *109*, 5620–5686.
(62) Agut, W.; Agnaou, R.; Taton, D.; Lecommandoux, S. *Macromol. Rapid Commun.* **2008**, *29*, 1147–1155.
(63) Ting, S. R. S.; Granville, A. M.; Quemener, D.; Davis, T. P.; Stenzel, M. H.; Barner-Kowollik, C. *Aust. J. Chem.* **2007**, *60*, 405–409.
(64) Lambert, J. B.; Shurvell, H. F.; Lightner, D. A.; Cooks, R. G., *Organic Structural Spectroscopy*; Prentice-Hall, Inc.: Upper Saddle River, NJ, 2001.
(65) Oh, S. Y.; Yoo, D. I.; Shin, Y.; Seo, G. *Carbohydr. Res.* **2005**, *340*, 417–428.
(66) Skoog, D. A. *Principles of Instrumental Analysis*, 6th ed.; Thomson Brooks/Cole: Belmont, CA, 2007.
(67) Stilbs, P. *Prog. Nucl. Magn. Reson. Spectrosc.* **1987**, *19*, 1–45.
(68) Cohen, Y.; Avram, L.; Frish, L. *Angew. Chem., Int. Ed.* **2005**, *44*, 520–554.
(69) Lauterbur, P. C. *Nature* **1973**, *242*, 190–191.
(70) Bihan, D. L., *Perfusion and Diffusion Magnetic Resonance Imagingn: Applications of Functional MRI*. Raven Press: New York, 1995.
(71) Gorman, C. B.; Smith, J. C.; Hager, M. W.; Parkhurst, B. L.; Sierzputowska-Gracz, H.; Haney, C. A. *J. Am. Chem. Soc.* **1999**, *121*, 9958–9966.
(72) Roberts, J. M.; Sierzputowska-Gracz, H.; Stejskal, E. O.; Osteryoung, J. G. *J. Phys. Chem. B* **1998**, *102*, 7735–7739.
(73) Derrick, T. S.; McCord, E. F.; Larive, C. K. *J. Magn. Reson.* **2002**, *155*, 217–225.
(74) Bleicher, K.; Lin, M.; Shapiro, M. J.; Wareing, J. R. *J. Org. Chem.* **1998**, *63*, 8486–8490.
(75) Price, K. E.; Lucas, L. H.; Larive, C. K. *Anal. Bioanal. Chem.* **2004**, *378*, 1405–1407.
(76) Hamblin, M. R.; Hasan, T. *Photochem. Photobiol. Sci.* **2004**, *3*, 436–450.
(77) Jori, G. *Anti-Infect. Agents Med. Chem.* **2007**, *6*, 119–131.
(78) Maisch, T.; Szeimies, R.-M.; Jori, G.; Abels, C. *Photochem. Photobiol. Sci.* **2004**, *3*, 907–917.
(79) Wainwright, M. *J. Antimicrob. Chemother.* **1998**, *42*, 13–28.
(80) Hancock, R. E. W. *Annu. Rev. Microbiol.* **1984**, *38*, 237–264.
(81) Brennan, P. J.; Nikaido, H. *Annu. Rev. Biochem.* **1995**, *64*, 29–63.
(82) Fu, L. M.; Fu-Liu, C. S. *Tuberculosis* **2002**, *82*, 85–90.
(83) Redl, F. X.; Lutz, M.; Daub, J. *Chem.—Eur. J.* **2001**, *7*, 5350–5358.
(84) Holzer, W.; Penzkofer, A.; Redl, F. X.; Lutz, M.; Daub, J. *Chem. Phys.* **2002**, *282*, 89–99.
(85) Ringot, C.; Sol, V.; Granet, R.; Krausz, P. *Mater. Lett.* **2009**, *63*, 1889–1891.
(86) Ringot, C.; Saad, N.; Granet, R.; Bressollier, P.; Sol, V.; Krausz, P. *J. Porphyrins Phthalocyanines* **2010**, *14*, 925–931.
(87) Ringot, C.; Sol, V.; Barriere, M.; Saad, N.; Bressollier, P.; Granet, R.; Couleaud, P.; Frochot, C.; Krausz, P. *Biomacromolecules* **2011**, *12*, 1716–1723.
(88) Drogat, N.; Granet, R.; Sol, V.; Le Morvan, C.; Begaud-Grimaud, G.; Lallouet, F.; Krausz, P. *Photodiagn. Photodyn. Ther.* **2011**, *8*, 157–157.
(89) Feese, E.; Ghiladi, R. A. *J. Antimicrob. Chemother.* **2009**, *64*, 782–785.
(90) Navarre, W. W.; Schneewind, O. *Microbiol. Mol. Biol. Rev.* **1999**, *63*, 174–229.
(91) Trias, J.; Benz, R. *Mol. Microbiol.* **1994**, *14*, 283–290.
(92) Ghose, T. K. *Pure Appl. Chem.* **1987**, *59*, 257–268.
(93) Gilkes, N. R.; Henrissat, B.; Kilburn, D. G.; Miller, R. C.; Warren, R. A. J. *Microbiol. Rev.* **1991**, *55*, 303–315.
(94) Beguin, P. *Annu. Rev. Microbiol.* **1990**, *44*, 219–248.
(95) Beguin, P.; Aubert, J. P. *FEMS Microbiol. Rev.* **1994**, *13*, 25–58.
(96) Varrot, A.; Leydier, S.; Pell, G.; Macdonald, J. M.; Stick, R. V.; Henrissat, B.; Gilbert, H. J.; Davies, G. J. *J. Biol. Chem.* **2005**, *280*, 20181–20184.
(97) Mba Medie, F.; Ben Salah, I.; Drancourt, M.; Henrissat, B. *Microbiology* **2010**, *156*, 1468–1475.